



Full Text View

[Volume 32, Issue 5 \(May 2002\)](#)
Journal of Physical Oceanography

 Article: pp. 1567–1573 | [Abstract](#) | [PDF \(531K\)](#)

Large-Amplitude Internal Solitary Waves in the North Equatorial Countercurrent

Peter Brandt
Institut für Meereskunde, Universität Kiel, Kiel, Germany
Angelo Rubino*
Institut für Meereskunde, Universität Hamburg, Hamburg, Germany
Jürgen Fischer
Institut für Meereskunde, Universität Kiel, Kiel, Germany

(Manuscript received March 29, 2001, in final form October 24, 2001)

DOI: 10.1175/1520-0485(2002)032<1567:LAI SWI>2.0.CO;2

ABSTRACT

The analysis of high-resolution oceanographic data referring to velocity measurements carried out by means of a vessel-mounted acoustic Doppler current profiler on 12 November 2000 in the equatorial Atlantic, at 44°W between 4.5° and 6°N, reveals the presence of three large-amplitude internal solitary waves superimposed on the velocity field associated with the North Equatorial Countercurrent (NECC). These waves were found in the deep ocean, more than 500 km off the continental shelf and far from regions of topographic variations. They propagated toward the north-northeast, strongly inclined with respect to the main axis of the NECC and perpendicular to the Brazilian shelf, as well as to the North Brazil Current, and were characterized by maximum horizontal velocities of about 2 m s^{-1} and maximum vertical velocities of about 20 cm s^{-1} . The large magnitudes of the measured velocities indicate that the observed waves represent disturbances evolving in a strongly stratified ocean. The distance separating the waves (about 70 km) indicates that the observed features cannot be considered as elements of a single train of internal solitary waves. The waves consist, instead, of truly disconnected, pulselike intense solitary disturbances. This behavior, which strongly differs from that typically observed for trains of tidally generated internal solitary waves, indicates that different mechanisms were possibly involved in their generation and/or evolution.

Table of Contents:

- [Introduction](#)
- [Collection of the data](#)
- [Observations](#)
- [Discussion](#)
- [REFERENCES](#)
- [TABLES](#)
- [FIGURES](#)

Options:

- [Create Reference](#)
- [Email this Article](#)
- [Add to MyArchive](#)
- [Search AMS Glossary](#)

Search CrossRef for:

- [Articles Citing This Article](#)

Search Google Scholar for:

- [Peter Brandt](#)
- [Angelo Rubino](#)
- [Jürgen Fischer](#)

1. Introduction

Oceanic large-amplitude internal solitary waves propagating along the near-surface waveguide over long distances are frequently observed in the World Ocean ([Ostrovsky and Stepanyants 1989](#); [Apel 1995](#)). Despite their ubiquity, the areas where the generation of large-amplitude internal solitary waves occurs are substantially restricted to coastal areas or to areas characterized by strong topographic variations influencing the near-surface flow field. This is due to the fact that only few mechanisms among those capable of exciting the internal, near-surface oceanic wave field seem to be efficient in generating large-amplitude internal solitary waves. In particular, these oceanic features, often observed as trains of rank-ordered disturbances, mainly arise from the disintegration of the internal tide generated by the interaction of a barotropic tidal flow with topographic features such as strait sills and continental slopes. However, there is also evidence that they can emerge from disturbances in the ambient near-surface current or density field caused by intrusions of buoyant waters of riverine or glacial origin or by coastal upwelling ([Apel 1995](#); [Vlasenko et al. 1998](#)). More widespread (i.e., not restricted to coastal areas) mechanisms that are able to excite the near-surface oceanic internal wave field derive, for example, from atmospheric (wind or pressure) fluctuations and geostrophic adjustment of the near-surface flow ([Munk 1981](#); [Munk and Wunsch 1998](#)). In particular, although geostrophic adjustment has not yet been proved to be capable of originating large-amplitude internal solitary waves in the deep ocean, it has been proved to induce internal solitary waves in laboratory experiments ([Hallworth et al. 2001](#)). This discrepancy may result from the fact that there is a very scarce source of highly ageostrophic currents in the deep ocean and that the oceanic phenomena from which such adjustment can derive are characterized by a huge variability in time and space. In the area of the North Brazil Current (NBC)/North Equatorial Countercurrent (NECC) retroflection zone highly nonstationary currents are encountered that derive from water masses crossing the equator within the NBC as well as from flow instabilities. In this area the presence of tidally generated trains of internal solitary waves has also been documented ([Kuznetsov et al. 1984](#)).



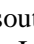


Here we report on observations of large-amplitude, pulselike internal solitary waves in the region occupied by the NECC and discuss their behavior in comparison to the behavior observed typically for trains of tidally generated internal solitary waves.

2. Collection of the data

In this study we use high-resolution velocity data, which were acquired with a 75-KHz phased-array acoustic Doppler current profiler (ADCP) named Ocean Surveyor (OS), during the RV *Sonne* cruise 151 (SO151) in November 2000. In particular, we analyze velocity data that are acquired along a northeastward oriented section from the coast of French Guiana to the Mid-Atlantic Ridge as well as along a southward oriented section along 44°W from the Mid-Atlantic Ridge to the Brazilian shelf just north of the equator. The OS was set up to send out acoustic pulses (pings) every four seconds and store the data as single-ping profiles. The data were collected using a vertical bin length of 16 m. In most of the surveyed area, good data (50% good criterion) were obtained to a depth range of 600 m during daytime and to a depth range of 500 m during nighttime. The range decreased slightly due to low scattering layers in the measurements close to the continental shelf of Brazil, in parts including the region of the NBC. Due to calm weather the vessel was very stable, and we estimate that the 1-min low-pass filtered horizontal velocity was measured with an accuracy better than 0.04 m s^{-1} after proper elimination of any transducer misalignment and using differential GPS data and heading information from an Ashtech 3D GPS. To check the validity of the vertical velocity, the so-called error velocity was analyzed. Two estimates of the vertical velocity are inferred from the two orthogonal back-to-back beams of an ADCP. The average between the two is the mean vertical velocity, presented in the following, and the difference is the error velocity. However, we found that maximum values of the 1-min low-pass filtered error velocity were in general much smaller than 0.1 m s^{-1} and, more important, no coherent signals could be found in the fields of error velocity; that is, the fields looked like random fields without spatial inhomogeneities, suggesting that any signal in the vertical velocity that is coherent over a large part of the water column should be reliable.


3. Observations

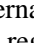
[Figure 1](#) shows the northward ([Fig. 1a](#)) as well as the eastward ([Fig. 1b](#)) component of the horizontal velocity field (the data represent averages between 30 and 78 m) as measured by the OS on 12 November 2000 at 44°W. Plotted are 1-min low-pass filtered velocity data. Between about 3.5° and 6°N strong eastward current velocities were detected, which can be associated with the NECC. A maximum core velocity of about 1.8 m s^{-1} was observed at about 5.1°N. In general, the observed velocity field shows undulations with length scales of $O(100 \text{ km})$. Superimposed on these undulations are several small-scale, pulselike disturbances. In particular, within the region occupied by the NECC, three sharp, well-distinguished peaks are evident in both velocity components. They are located about 70 km apart, the northernmost one being located at about 5.9°N. The values of the maximum horizontal velocity anomalies as well as other parameters characterizing these disturbances are given in [Table 1](#). Assuming that the Coriolis force can be neglected on the length scales characterizing the observed disturbances, the direction along which the observed waves propagate is given by the direction of the maximum horizontal velocity anomaly. For all three waves, this direction is about north-northeast and therefore strongly inclined (about 60 to 65 deg) with respect to the main axis of the NECC, which flows eastward.

During the passage of the ship through the three waves, sharply defined bands of increased surface roughness with breaking surface waves were observed visually, which led also to strong signals on the ship radar. Unfortunately, recording of ship radar data was not possible during the cruise and high-resolution satellite data were unavailable. A detailed view of the horizontal as well as the vertical velocity structure within the three disturbances is presented in [Fig. 2](#) , in which the velocity data are plotted as a function of time. The Doppler shift inherent in the observed data was estimated using the (known) ship velocity as well as an estimate of the phase velocity (2.5 m s^{-1}) that was obtained from the Miyata equations ([Miyata 1988](#)) using a first-mode linear internal wave phase speed inferred by the observed stratification and an estimate of the wave amplitude. The obtained horizontal length scales are given in the upper panels of [Fig. 2](#) . The northward components of the horizontal velocity field associated with the three waves are very similar in strength and structure. On the contrary, the eastward components are quite different. In particular, wave **a** marks a transition region between NECC and undisturbed ocean: while in front of wave **a** (north of it) the eastward velocity is about zero, this velocity is significantly larger (about 0.2 m s^{-1} averaged between 30 and 78 m; see also [Fig. 1](#) ) in its rear (south of it). Wave **b** is located entirely within the NECC, but it also marks, like in the previous case, a transition region. In front of wave **b** smaller eastward velocities (about 0.8 m s^{-1} averaged between 30 and 78 m; see also [Fig. 1](#) ) are encountered than in its rear (about 1.2 m s^{-1} ; see also [Fig. 1](#) ). The thickness of the NECC is maximum in the location occupied by wave **c**. There eastward velocities greater than 1 m s^{-1} are encountered in the upper 120 m of the water column. Note that in the eastward as well as in the vertical component of the velocity fields the maximum anomalies associated with the internal waves deepen from wave **a** to wave **c**. As stated before, this behavior cannot be detected in the northward component of the velocity field.

The horizontal as well as the vertical velocity fields of each wave show the typical structure associated with internal gravitational solitary waves. The shapes of the isolines of the northward velocity component (or, equivalently, of the horizontal velocity anomalies) are in fact nearly semi-elliptical, and those of the vertical velocity component nearly antisymmetric. The fronts of the waves are associated with downward velocities and the rears with upward velocities, their maximum amplitude being about 20 cm s^{-1} . These characteristics of the observed features agree qualitatively with those of large-amplitude internal solitary waves described theoretically and observed in high-resolution measurements (see, e.g., [Vlasenko et al. 2000](#)).

4. Discussion

An overview of the shallow current branches in the NBC/NECC retroflexion zone (the data refer to depth averages between 60 and 125 m) superimposed on the chlorophyll concentration observed by the Sea-Viewing Wide Field-of-View Sensor (SeaWiFS) aboard the *SeaStar* satellite during November 2000 is given in [Fig. 3](#) . In particular, using the data acquired along two sections oriented almost perpendicular to the coast that merge at the Mid-Atlantic Ridge, the structure of the NBC retroflexion can be elucidated. At 44°W the NBC is mainly confined to the local steep shelf break, its maximum velocity being about 1 m s^{-1} . Note, however, that some weaker flow extends offshore over nearly 300 km distance. Farther northwest, off French Guiana (near 53°W), the currents at the shelf break turn offshore and then eastward at about 9°N . However, the chlorophyll distribution reveals that the change in the observed current direction represents an eddy released by the NBC. As discussed before, at 44°W we observed a fully developed NECC in the latitude band from 3.5° to about 6°N .

In [Fig. 3](#)  the maximum velocity anomalies associated with the three large-amplitude internal solitary waves described in the previous section are also shown. The waves propagate toward the north-northeast, in a region of deep water (even in the region characterized by the topographic variations associated with the Sierra Rise the water depth exceeds 3000 m). Assuming that they were generated at the steep Brazilian shelf break (which could be compatible with a tidal generation mechanism), they should have traveled about 500 km to reach the location where they were observed.

Despite the absence of topographic constrictions in the region, which could allow for wave energy focusing, the tidal generation mechanisms along the Brazilian continental shelf (i.e., a line source mechanism) could still be effective in producing large-amplitude internal solitary waves, especially if the waves are amplified by wave-current interaction occurring across frontal regions with strong horizontal density gradients ([Kuznetsov et al. 1984](#)). The distance separating the waves (about 70 km) indicates that the observed features cannot be considered as elements of a single train of internal solitary waves as, for waves having similar amplitudes (and hence similar phase speeds), it would take an unrealistically large distance to obtain the observed separation distance. The waves consist, instead, of truly disconnected pulselike intense solitary disturbances. Neglecting the advection due to the NECC, which is almost perpendicular to the direction of wave propagation, it is possible to calculate from the estimate of the phase speed c_{ph} , the direction of propagation α , and the separation in space, Δs , and time, Δt , the period of internal wave generation T according to

$$T = \frac{\Delta s \cos \alpha}{c_{ph}} + \Delta t. \quad (1)$$

The resulting periods of $T = 11.4$ h for waves **a/b** as well as $T = 13.8$ h for waves **b/c** are close to the semidiurnal tidal period, which strengthens the hypothesis of a tidal generation mechanism.

The fact that such a mechanism can be efficient in equatorial regions is confirmed by [Pinkel \(2000\)](#), who observed tidally generated internal solitary waves in the western equatorial Pacific Ocean. However, in contrast to our measurements, the trains of solitary waves that he observed were clearly composed of rank-ordered elements and the peak velocities of the single waves were much smaller (about 80 cm s^{-1}).

In [Fig. 4](#) the eastward component of the current field associated with the NECC is depicted. The velocity data were interpolated onto a regular grid by objective mapping using horizontal scales of 10 km and vertical scales of 40 m. Thus, the currents appear much smoother than in the original resolution. Nevertheless, the eastward flowing NECC centered at 5.1°N still shows 1.6 m s^{-1} currents near the surface. Large horizontal and vertical shears are associated with this current. To assess the nonlinearity inherent in this jet, the relative vorticity estimated by the zonal variation of the eastward velocity component $\partial U/\partial y$ scaled by the planetary vorticity f is shown above the contoured isotachs. Note that, for this calculation, the flow (depth averaged between 60 and 125 m) was filtered over a 100-km length scale. This quantity can be interpreted as a local Rossby number and, because it is close to unity at both sides of the jet, it indicates that the NECC has a large ageostrophic component. In conclusion, aspects of the behavior of the observed internal solitary waves strongly differ from that typically observed for trains of tidally generated internal solitary waves. This, though not excluding that they are of tidal origin (as their separation distance would suggest), indicates that different mechanisms were possibly involved in their generation and/or evolution.

Acknowledgments

We thank the captain and crew of the RV *Sonne* for their help, M. Müller and U. Papenburg for their technical assistance, and V. Vlasenko for helpful discussions. The OS was kindly provided by the manufacturer RD Instruments, San Diego, California, for the RV *Sonne* cruises SO151–SO153. We would like to express our gratitude to E. Firing who equipped us with software for processing the OS raw data. The chlorophyll data are provided by the SeaWiFS Project, NASA/Goddard Space Flight Center, and ORBIMAGE. Financial support was obtained by the Bundesminister für Bildung und Forschung, Bonn, Germany, under Grant 03G0151A.

REFERENCES

- Apel J. R., L. A. Ostrovsky, and Yu. A. Stepanyants, 1995: Internal solitons in the ocean. Tech. Rep. MERCJRA0695, 70 pp. [Available from Milton S. Eisenhower Research Center, Applied Physics Laboratory, The Johns Hopkins University, Johns Hopkins Rd., Laurel, MD 20707.].
- Hallworth M. A., H. E. Huppert, and M. Ungarish, 2001: Axisymmetric gravity currents in a rotating system: Experimental and numerical investigations. *J. Fluid Mech.*, **447**, 1–29. [Find this article online](#)
- Kuznetsov A. S., A. N. Paramonov, and Yu. A. Stepanyants, 1984: Investigation of solitary internal waves in the tropical zone of the western Atlantic. *Izv. Acad. Sci. USSR Atmos. Oceanic Phys.*, **20**, 840–846. [Find this article online](#)
- Miyata M., 1988: Long internal waves of large amplitude. *Nonlinear Water Waves*, K. Horikawa and H. Maruo, Eds., Springer-Verlag, 399–406.
- Munk W. H., 1981: Internal waves and small-scale processes. *Evolution of Physical Oceanography*, B. A. Warren and C. Wunsch, Eds., The MIT Press, 264–291.
- Munk W. H., and C. Wunsch, 1998: Abyssal recipes II: Energetics of tidal and wind mixing. *Deep-Sea Res.*, **45**, 1977–2010. [Find this article online](#)
- Ostrovsky L. A., and Yu. A. Stepanyants, 1989: Do internal solitons exist in the ocean? *Rev. Geophys.*, **27**, 293–310. [Find this article online](#)
- Pinkel R., 2000: Internal solitary waves in the warm pool of the western equatorial Pacific. *J. Phys. Oceanogr.*, **30**, 2906–2926. [Find this article online](#)
- Vlasenko V. I., V. A. Ivanov, A. D. Lisichenok, and I. G. Krasin, 1998: The generation of intensive short-period internal waves in the

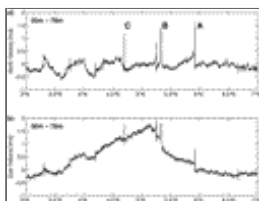
Tables

TABLE 1. Values of different parameters characterizing the large-amplitude internal solitary waves measured by the OS on 12 Nov 2000 at 44°W

Characteristic	Wave A	Wave B	Wave C
Max northward velocity anomaly (m s ⁻¹)	1.7	1.57	1.4
Max eastward velocity anomaly (m s ⁻¹)	0.87	0.96	0.63
Propagation direction (° from north)	27	21	24
Max downward velocity (m s ⁻¹)	-0.23	-0.14	-0.25
Max upward velocity (m s ⁻¹)	0.18	0.13	0.13
Latitude (°N)	5.92	5.33	4.69
Time (UTC)	1009	1522	2209

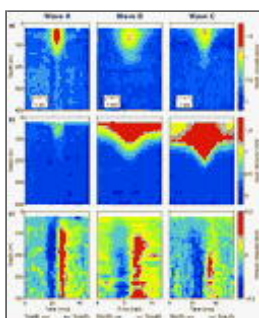
[Click on thumbnail for full-sized image.](#)

Figures



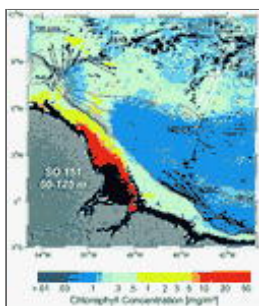
[Click on thumbnail for full-sized image.](#)

FIG. 1. Northward (a) as well as eastward (b) component of the horizontal velocity field as measured by the OS on 12 Nov 2000 at 44°W as function of latitude. The data represent 1-min low-pass filtered velocity data averaged between 30- and 78-m depth. The three large amplitude waves discussed in the following sections are marked by **a**, **b**, and **c**





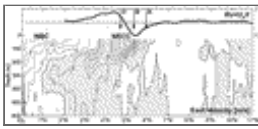
[Click on thumbnail for full-sized image.](#)

FIG. 2. Northward (a), eastward (b), and vertical (c) component of the velocity field for the three waves **a**, **b**, and **c** as a function of time and depth. The horizontal length scales given in (a) were obtained by estimating the Doppler shift inherent in the observed data from the known ship velocity as well as from an estimate of the phase velocity




[Click on thumbnail for full-sized image.](#)

FIG. 3. Geographical map of the western tropical Atlantic including the NBC/NECC retroflection zone with the near-surface current vectors (the data are depth averaged between 60- and 125 m) measured during RV *Sonne* cruise SO151 superimposed on chlorophyll concentration measured by SeaWiFS aboard the *SeaStar* satellite. The white arrows refer to the maximum velocity anomalies (given in [Table 1](#) ) corresponding to the waves marked by **a**, **b**, and **c** in [Fig. 1](#) 



[Click on thumbnail for full-sized image.](#)

FIG. 4. Eastward component of the velocity field as a function of latitude and depth. A local Rossby number (thick solid line), as well as the positions of waves **a**, **b**, and **c** (see [Fig. 1](#) ) is shown above the contoured isotachs

* Current affiliation: Dipartimento di Scienze Ambientali dell' Università Ca' Foscari di Venezia, Venice, Italy

Corresponding author address: Peter Brandt, Institut für Meereskunde an der Universität Kiel, Düsternbrooker Weg 20, 24105 Kiel, Germany. E-mail: pbrandt@ifm.uni-kiel.de

[top](#) ▲



© 2008 American Meteorological Society [Privacy Policy and Disclaimer](#)
Headquarters: 45 Beacon Street Boston, MA 02108-3693
DC Office: 1120 G Street, NW, Suite 800 Washington DC, 20005-3826
amsinfo@ametsoc.org Phone: 617-227-2425 Fax: 617-742-8718
[Allen Press, Inc.](#) assists in the online publication of AMS journals.